ACS SENSORS

ACS Editors' Choice

Article

Cite This: ACS Sens. 2019, 4, 883–891

pubs.acs.org/acssensors

pH-Lemon, a Fluorescent Protein-Based pH Reporter for Acidic Compartments

Sandra Burgstaller,*[,†] Helmut Bischof,*[,†] Thomas Gensch,[‡] Sarah Stryeck,[†] Benjamin Gottschalk,[†] Jeta Ramadani-Muja,[†] Emrah Eroglu,[†] Rene Rost,[†] Sabine Balfanz,[‡] Arnd Baumann,[‡] Markus Waldeck-Weiermair,*[,†] Jesse C. Hay,[†,§] Tobias Madl,[†,∥] Wolfgang F. Graier,*[,†,∥] and Roland Malli*[,†,∥]

[†]Molecular Biology and Biochemistry, Gottfried Schatz Research Center, Medical University of Graz, Neue Stiftingtalstraße 6/6, 8010 Graz, Austria

[‡]Institute of Complex Systems, Zelluläre Biophysik (ICS-4), Forschungszentrum Jülich, 52428 Jülich, Germany

[§]Division of Biological Sciences and Center for Structural and Functional Neuroscience, The University of Montana, 32 Campus Drive, HS410, Missoula 59812-4824, Montana United States

[∥]BioTechMed Graz, Mozartgasse 12/II, 8010 Graz, Austria

Supporting Information

ABSTRACT: Distinct subcellular pH levels, especially in lysosomes and endosomes, are essential for the degradation, modification, sorting, accumulation, and secretion of macromolecules. Here, we engineered a novel genetically encoded pH probe by fusing the pH-stable cyan fluorescent protein (FP) variant, mTurquoise2, to the highly pH-sensitive enhanced yellow fluorescent protein, EYFP. This approach yielded a ratiometric biosensor—referred to as pH-Lemon—optimized for live imaging of distinct pH conditions within acidic cellular compartments. Protonation of pH-Lemon under acidic conditions significantly decreases the yellow fluorescence while the cyan fluorescence increases due to reduced Förster resonance energy transfer (FRET) efficiency. Because of its freely reversible and ratiometric responses, pH-Lemon represents a fluorescent biosensor for pH dynamics. pH-Lemon also shows a sizable pH-dependent fluorescence lifetime change that can be used in fluorescence lifetime imaging microscopy as an alternative observation method for the study of pH in acidic cellular compartments. Fusion of pH-Lemon to the protein microtubule-associated protein 1A/1B-light chain 3B (LC3B), a specific marker of autophagic membranes, resulted in its targeting within autolysosomes of HeLa cells. Moreover, fusion of pH-Lemon to a glycophosphatidylinositol (GPI) anchor allowed us to monitor the entire luminal space of the secretory pathway and the exoplasmic leaflet of the plasma membrane. Utilizing this new pH probe, we revealed neutral and acidic vesicles and substructures inside cells, highlighting compartments of distinct pH throughout the endomembrane system. These data demonstrate, that this novel pH sensor, pH-Lemon, is very suitable for the study of local pH dynamics of subcellular microstructures in living cells.

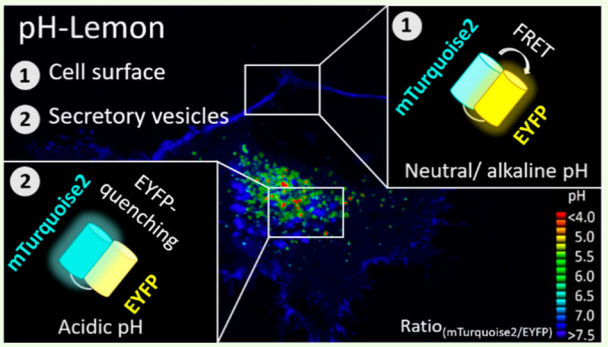

KEYWORDS: *array confocal laser scanning microscopy, FLIM, fluorescence microscopy, FRET, genetically encoded probes, Golgi apparatus, GPI-anchor, pH*

Even small pH changes impact protein structures to regulate diverse molecular processes such as enzymatic activities,[1] transporters,[2,3] ion channels,[4−6] and transcription,[7] which eventually determine cell functions. While most biological processes operate optimally at a narrow pH range between pH 7.2 and pH 7.4,[8,9] some require an alkaline or even acidic environment.[10,11] For the decomposition of pathogens,[12] self-digestion in the course of autophagy, as well as protein processing in the endomembrane system,[13] all cells contain highly acidic compartments such as lysosomes and endosomal vesicles with assumed pH values between pH 4.0 and pH 6.0, respectively.[14−16] Vacuolar-type H^+-ATPases[17] (V-ATPases) pump H^+ across biomembranes of these compartments to acidify their lumens. A loss of these H^+ gradients is associated with severe dysfunctions.[18] Given the importance of acidic cellular organelles,[19−21] the development and optimization of pH probes for real-time visualization of pH dynamics is an active research area.[22] Several organic small molecule fluorophores have been developed to label acidic

Received: December 14, 2018
Accepted: March 13, 2019
Published: March 13, 2019

vesicles within cells.[23−25] However, most of these compounds might be cytotoxic and alter the metabolic activity of cells.[25] Moreover, these dyes are released from vesicles upon deprotonation, thus hampering quantification of actual pH levels and dynamics.[25] A more elegant way to assess (sub)cellular pH levels is the application of nontoxic genetically encoded fluorescent biosensors.[26,27] The first FP-based pH biosensor was developed by introducing site specific mutations to a GFP variant which increased its natural pH sensitivity.[26] Miesenböck and colleagues invented and successfully applied these "pHlourins"[26] to visualize local pH changes within vesicles during secretion and synaptic transmission. These pH-sensors, however, are best suited for pH measurements near neutral pH and have very low sensitivity at and below pH 6.0. Another informative type of genetically encoded fluorescent pH sensors is Cy11.5 and pHlameleons.[27] These biosensors consist of the enhanced cyan FP (ECFP)[28] with sizable fluorescence at acidic pH directly fused to a yellow FP variant (YFP).[29] The pHlameleons are ratiometric FRET-based pH probes that have been characterized in detail as recombinant probes *in vitro*.[27] Cytosolic pHlamelons were also characterized for both ratiometric and lifetime pH imaging in live CHO, PC12, and MCF7 cells. Furthermore, the probes were used to quantify small cytosolic pH changes in response to N-dodecyl (C12) imidazole, a lysosomotropic detergent. However, pHlameleons have yet not been targeted to cellular organelles such as mitochondria, endosomes, or lysosomes.[27] Worth noting, a pHlameleon-like FRET-based pH-sensor family, FluBpH, has been introduced recently, where a flavin-binding fluorescent protein (FbFP) replaces ECFP as a donor, thus eliminating the problem of the pH-dependence of ECFP fluorescence at pH values below 6.5.[30] In this study, we used the pHlameleon principle to design a FRET-based pH biosensor using one of the most pH stable cyan FP variants, mTurquoise2,[31] fused to the highly pH sensitive EYFP.[29] We named this pHlameleon variant pH-Lemon and tested its applicability for imaging the pH of acidic vesicles by fusing it to LC3B or targeting it to the secretory pathway. These approaches demonstrated the suitability of pH-Lemon to detect and study neutral as well as acidic vesicles in intact living cells under various conditions using high-resolution fluorescence microscopy.

EXPERIMENTAL SECTION

Buffers and Solutions. Materials used for cell culture were purchased from Greiner Bio-One (Kremsmünster, Austria). Restriction enzymes, chemically competent 10-beta *Escherichia coli* (*E. coli*) cells for cloning and chemically competent BL21 (DE3) *E. coli* cells for protein expression were obtained from New England Biolabs (Ipswich, MA, USA). Agar−Agar Kobe I, $CaCl_2$, D-Glucose, HEPES, KCl, $MgCl_2$, NaCl, NaOH, Triton X-100, Trypton/Pepton, and Yeast extract were purchased from Carl Roth (Graz, Austria). Agarose was obtained from VWR International (Vienna, Austria). Lysis buffer (in mM): 100 Na_2HPO_4, 200 NaCl, 10 imidazole, 250 units of Benzonase Nuclease, and bacterial Protease Inhibitor Cocktail, pH 8.0. Buffer formulations were as follows: Washing buffer (in mM): 100 Na_2HPO_4, 200 NaCl, 40 Imidazole, pH 8.0. Purification buffer (in mM): 100 Na_2HPO_4, 200 NaCl, 200 imidazole, pH 8.0. Elution buffer (in mM): 10 HEPES, 0.05% Triton X-100, pH 7.3 with *N*-Methyl-D-glucamin (NMDG). Characterization of pH-Lemon *in vitro* was performed using elution buffers with different pH values adjusted, either with HCl or with NMDG. MES was used for the adjustment of pH values below 5.5 and MOPS was used for pH values above 9.0. The physiological buffer used for fluorescence microscopy experiments contained (in mM): 138 NaCl, 5 KCl, 2 $CaCl_2$,1 $MgCl_2$, 10 D-glucose, pH adjusted to 7.4 with NaOH (referred to as "2Ca"). EC_{50} values *in situ* were determined using a physiological buffer with different pH, containing either (in mM) 10 MES (for adjustment of pH < 5.5), 10 HEPES (pH 5.5−9.0) or 10 MOPS (pH > 9.0); pH was adjusted using HCl or NaOH. For calcium measurements, cells were equilibrated and incubated in EHL-buffer (in mM): 2 $CaCl_2$, 135 NaCl, 1 MgCl, 5 KCl, 10 Hepes, 2.6 $NaHCO_3$, 0.44 KH_2PO_4, 0.34 Na_2HPO_4, 1× amino acids, 1× vitamins, 10 glucose, and 2 L-glutamine with a pH of 7.45. For wide-field imaging of calcium signals, the physiological buffer was modified (in mM): 138 NaCl, 5 KCl, 0.1 EGTA, 1 $MgCl_2$, 10 D-glucose, pH adjusted to 7.4 with NaOH (referred to as "EGTA" in wide-field measurements). Adenosine 5′-triphosphate disodium salt (ATP) was purchased from Carl Roth (Graz, Austria). Neutralization buffer was composed of "2Ca"-buffer with 0.5% NaN_3 (Sigma-Aldrich, Vienna, Austria) and 50 mM NH_4Cl (Sigma-Aldrich, Vienna, Austria), pH adjusted to 9.0. Bafilomycin-A was purchased from Sigma-Aldrich.

Cloning. The cloning of differently targeted pH-probes was performed using standard cloning protocols provided by the manufacturer. Primers and cloning steps are described in more detail in the SI (page S-2).

Cell Culture and Transfection. HeLa and HEK-293 cells were cultured in DMEM containing 10% FCS, 100 U mL^{-1} penicillin, 100 $\mu g\ mL^{-1}$ streptomycin, and 2.5 $\mu g\ mL^{-1}$ Fungizone (Thermo Fisher Scientific). For the cultivation of INS-1 832/13 (INS-1) cells, Gibco RPMI 1640 media (ThermoFisher) was used. All cell types were cultivated in a humidified incubator (37 °C, 5% CO_2). To transfect HeLa cells, PolyJet (SignaGen Laboratories, Rockville, USA) was used as transfection reagent 48 h prior to measurements according to manufacturer's protocol. For transfection of INS-1 and HEK-293 cells, TransFast transfection reagent (Promega, Madison, USA) was used. Transfections using TransFast were performed using 1.5 μg plasmid DNA and 2.5 μL TransFast per milliliter. After 4 h, media was replaced with fresh DMEM or Gibco RPMI 1640 media. HEK-293 cells for FLIM imaging were transfected using a modified calcium-phosphate method (for more details see SI page S-2).

Recombinant Protein Expression and Purification. Protein expression was induced by adding 1 mM β-D-1-thiogalactopyranoside (IPTG) at an OD600 of 0.8. Cell pellets were resuspended in 20 mL lysis buffer, followed by sonication (QSONICA Ultrasonic Processor; 12 min, 50% amplitude, 1 s on/off) for cell lysis. Centrifugation at 12 000 rpm for 45 min at 4 °C (Sorvall LYNX 6000) and filtration (0.45 μm cellulose acetate syringe filters) was used to clear the lysates. 5 mL HisTrap columns (GE Healthcare, Vienna, Austria) for immobilized metal affinity chromatography on an ÄKTA pure system (GE Healthcare, Vienna, Austria) were used to purify the proteins. HisTrap columns were equilibrated using lysis buffer. Cleared *E. coli* lysates were applied to the columns at a flow rate of 2 mL min^{-1} and contaminants were removed using washing buffer. Finally, proteins were eluted with purification buffer. Proteins were further purified at room temperature using size exclusion columns (10/300 200 pg, GE Healthcare) on an ÄKTA pure system (GE Healthcare) with SEC buffer. Finally, protein concentration was calculated using absorbance at 280 nm, determined by NanoDrop 1000 UV/vis spectrometer (Thermo Fisher Scientific, Vienna, Austria).

Characterization of Recombinant pH-Lemon Variants. The purified proteins were analyzed using the CLARIOstar plate reader (BMG Labtech, Ortenberg, Germany). All proteins were used at a final concentration of 200 nM. To generate the EC_{50} curve and test the temperature dependency of the recombinant proteins *in vitro*, samples were analyzed using FRET (excitation at 430 nm ± 10 nm, emission at 475 nm ± 10 nm/dichroic mirror: 452.5 nm and emission at 525 nm ± 10 nm/476.2 nm) and single fluorescent protein fluorimetry (excitation at 430 nm ± 10 nm and 480 nm ± 10 nm, emissions at 475 nm ± 10 nm/452.5 and 525 nm ± 10 nm/501.2 nm). FRET-spectra scans were performed using an excitation of 413.4 nm ± 8 nm and emission was observed sequentially from 450 to 550 nm, where the center wavelength of a 5 nm broad spectral observation window was shifted with a step width of 1 nm. Gain was set to 2000. EYFP spectra were generated using excitation at 480 nm ± 8 nm and

DOI: 10.1021/acssensors.8b01599
ACS Sens. 2019, 4, 883−891

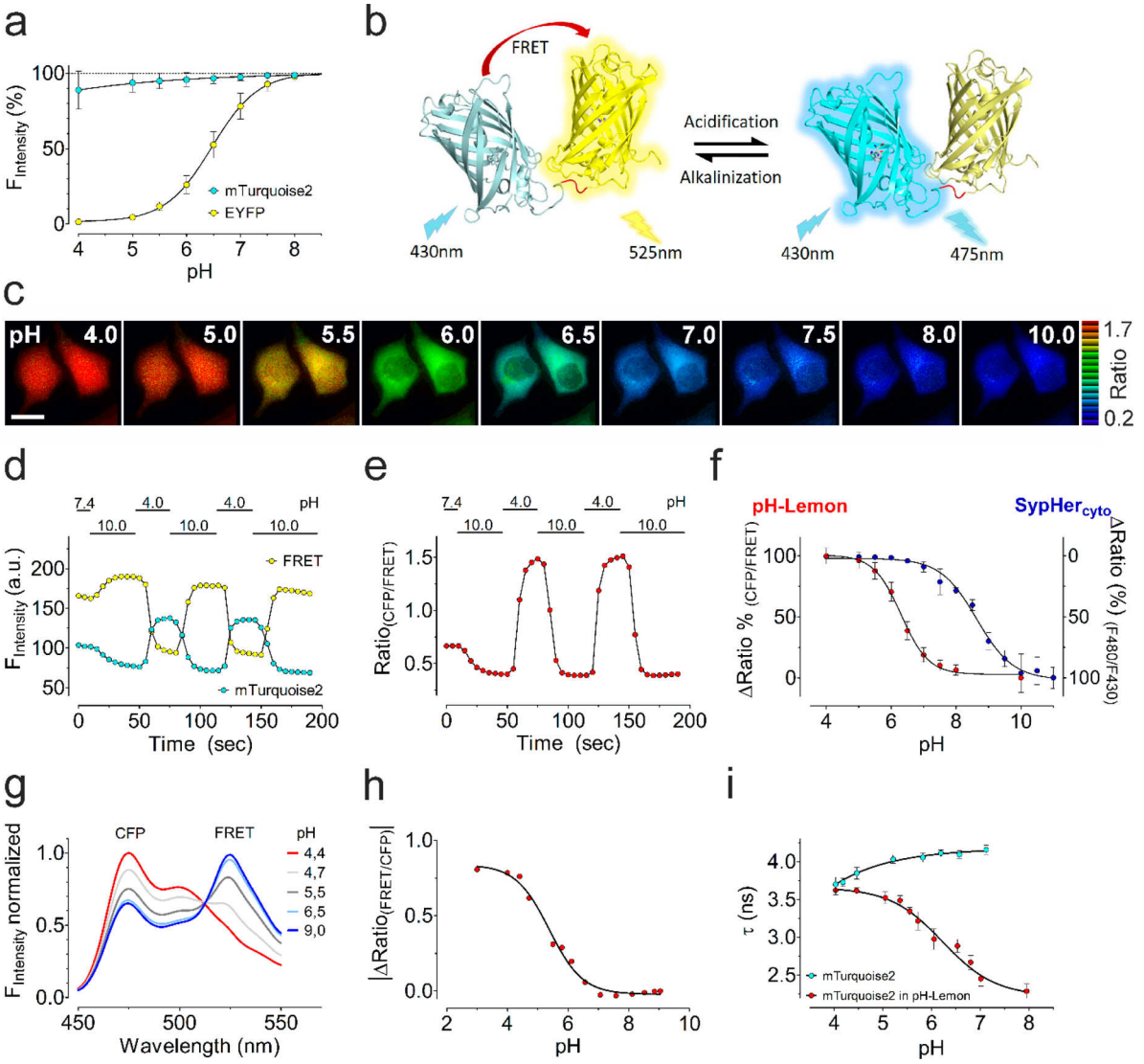

Figure 1. Characterization of mTurquoise2, EYFP, and pH-Lemon in cells and *in situ* (a–f) and *in vitro* (g–i). (a) Impact of pH on the fluorescence intensities of mTurquoise2 and EYFP. The two FPs were separately expressed in the cytosol of HeLa cells and the fluorescence intensities in different pH-environments were measured upon cell permeabilization using nigericin and monensin. Data represent average ± SD, n = 3 independent experiments for EYFP, n = 4 independent experiments for mTurquoise2. (b) Sensor scheme of pH-Lemon, a fusion construct of mTurquoise2 and EYFP, which are connected via a flexible linker (red line). (c) Representative pseudocolored wide-field fluorescence ratio (mTurquoise2/FRET) images of HeLa cells expressing cytosolic pH-Lemon at different pH values. Scale bar represents 10 μm. (d) Donor (cyan) and FRET (yellow) intensities of pH-Lemon expressed in HeLa cells upon repetitive switching between pH 4 and pH 10 after cell permeabilization. (e) Respective FRET ratio curve over time according to panel (d). (f) Concentration response curve (CRC) of pH-Lemon (n = 3, average ± SD) and SypHer (n = 3, average ± SD), a single FP-based pH probe with a higher pK_a-value *in situ*. (g) Emission FRET-spectra of purified pH-Lemon at different pH values *in vitro*. (h) CRC of purified pH-Lemon *in vitro* (n = 3 ± SD). (i) Representative fluorescence lifetimes of mTurquoise2 alone (cyan circles) or mTurquoise2 as FRET donor within pH-Lemon (red circles) at different pH. Data represents average ± SD of 3–58 cells per pH.

emission from 510 to 580 nm where the center wavelength of a 5 nm broad spectral observation window was shifted with a step width of 1 nm. Spectra were normalized for area under the curve.

Live Cell Imaging. Wide-field live cell imaging was performed at an inverted and advanced fluorescent microscope using a 40× or a 100× magnification objective (EC Plan-NEO FLUAR 40×; alpha Plan FLUAR 100×, Zeiss, Göttingen, Germany) with a motorized sample stage (TILL Photonics, Gräfelfing, Germany). The microscope was equipped with the charge-coupled device camera AVT Stingray 25 F145B (Allied Vision Technologies, Stadtroda, Germany). Prior to the measurements cells were equilibrated in storage buffer for 30 min. During the experiment, buffers were exchanged using a flow chamber, connected to a gravity-based perfusion system (NGFI, Graz, Austria) and a vacuum pump (Chemistry diaphragm pump ME 1c, Vacuubrand, Wertheim, Germany). FRET imaging was performed using excitation at 430 nm and emissions at 475 and 525 nm. For single fluorescent protein fluorimetry, CFP and YFP were excited at 430 and 500 nm, respectively. Emissions were collected at 475 and 525 nm. The software Live acquisition 2 (TILL Photonics) was used for acquisition. High resolution imaging was performed using a Nipkow-disk-based array confocal laser scanning microscope (ACLSM). The ACLSM consisted of a Zeiss Axiovert 200 M (Zeiss Microsystems, Jena, Germany) with a 100× objective (α Plan-Fluar 100×/1.45 oil objective, Zeiss Microsystems, Jena, Germany), equipped with VoxCell Scan (VisiTech, Sunderland, UK), and an air cooled argon ion laser system (series 543, CVI Melles Griot, CA, USA). The fluorescent proteins were illuminated sequentially using

DOI: 10.1021/acssensors.8b01599
ACS Sens. 2019, 4, 883–891

415 nm (CFP) and 510 nm (YFP) laser light. Emissions were collected at 475 and 525 nm using a CCD camera (CoolSnap HQ2, Photometrics, Tucson, Arizona, USA) and a binning of 2. For buffer exchange a gravity-based perfusion system (NGFI, Graz, Austria) was used. For cytosolic Ca^{2+} measurements cells were excited at 340 and 380 nm and emission of Fura-2 was collected at 510 nm.

Fluorescence Lifetime Imaging Microscopy *in Situ*. Fluoresence lifetime imaging (FLIM) was performed on an upright fluorescence microscope (A1MP; Nikon, Amsterdam, The Netherlands) equipped with a water immersion objective (25×; NA1.1; WD 2 mm; Nikon). Two-photon excitation of the pH-Lemon donor mT2 was achieved by a train of 100 fs light pulses (λ_{exc} = 880 nm; 80 MHz; Mai Tai DeepSee HP, Newport Spectra Physics; Irvine, CA). Fluorescence was detected with a GaAsP hybrid photodetector (HPM-100−40; Becker & Hickl, Berlin, Germany) after passing a bandpass filter at 445 ± 45 nm (445BP90, Omega Optical, Brattleboro, VT, USA). Fluorescence intensity decays were generated in every pixel of the image using multidimensional time-correlated single photon counting (TCSPC) employing TCSPC electronics (SPC-152; Becker & Hickl). FLIM images were generated using SPCImage 6.1 (Becker & Hickl) by plotting the amplitude weighted average fluorescence lifetime tau_ave as color-coded value. tau_mean was obtained from iterative least-squares minimizing based fitting routine of a biexponential fitting function which was reconvoluted with the instrument response function to describe the time course of the pixel fluorescence intensity decays properly.

Fluorescence Lifetime Imaging Spectroscopy *in Vitro*. Fluorescence lifetimes of purified pH-Lemon expressed in *E. coli* were also determined from time-resolved fluorescence measurements using a time-resolved fluorescence spectrophotometer (Fluotime 100; Picoquant; Berlin; Germany) based on a PicoHarp300 unit (TCSPC-based), with a pulsed diode laser (LDHC440; λ_{exc} = 440 nm; 50 ps pulse width; 20 MHz repetition frequency) as excitation source and a photomultiplier for single photon detection. Donor and acceptor emission of pH-Lemon was selected at 475 and 530 nm, respectively, by applying a monochromator.

Calibration of pH-Lemon - cyto. HeLa cells were permeabilized using 5 μM nigericin (Tocris, Abingdon, United Kingdom) and 10 μM monensin (Sigma-Aldrich, Vienna, Austria). The intracellular pH was adjusted via perfusion of an extracellular experimental buffer with distinct pH values.

Calibration of pH-Lemon - GPI. HeLa cells were perfused with an extracellular buffer with pH 4.0 and 10.0 representing the minimum and maximum of the sensor. Respective maximal and minimal ratio signals of the cell surface of single cells were used to define pH values according to the formula shown in SI on page S-2.

Starvation of Cells. For autophagy induction, cells were washed with PBS twice to remove the nutrients and starved for at least 1 h in nutrient free salt-buffer solution ("2Ca-buffer").

Neutralization of Endosomal Vesicles. Vesicles were either neutralized using incubation with neutralization buffer (see Buffers and Solutions) for 5 min or preincubation with 0.5 μM bafilomycin-A in DMEM for 70 min at 37 °C (for the subsequent experiments, Baf-A was present in every buffer).

Co-Localization of pH-Lemon with mCherry-Golgi-7. Cells were cotransfected with pH-Lemon and mCherry-Golgi-7, which was a gift from Michael Davidson (Addgene plasmid # 55167). For cell fixation, HeLa cells were washed 3 times with PBS, followed by 10 min incubation at room temperature with 3.7% paraformaldehyde (PFA). After 3 additional washing steps, cells were kept in PBS for imaging.

Cytosolic Ca^{2+} Measurements. For the measurement of cytosolic Ca^{2+} levels, HeLa cells were washed 3 times with EHL-buffer and then loaded with 3.3 μM Fura-2 AM in EHL-buffer for 45 min. After washing several times with EHL-buffer, cells were measured using wide-field microscopy. 100 μM ATP was used as an IP_3-generating agonist in "2 Ca"- or "EGTA"- buffer for Ca^{2+} mobilization.

Acidic Compartment Staining. LysoTracker Red DND-99 (ThermoFisher, Vienna, Austria) was used for 30 min at 37 °C at a final concentration of 75 nM.

Data Analysis. Obtained data were analyzed using Excel (Microsoft), MetaMorph (Molecular devices), and GraphPad Prism 5 Software (GraphPad Software, Inc., La Jolla, CA, USA). Pseudocolored ratio images were generated using MetaMorph software. Ratio scale was set as demonstrated in the figures. For data visualization, CorelDraw was used. Images generated using ACLSM were adjusted in light and contrast (+40/+40%). For the calculation of the EC_{50} values, the FRET (or YFP) fluorescence was divided by the mTurquoise2 fluorescence (Figure 1h,i, Figure S1c, and Figure 2b). Since 100% of the EYFP fluorescence were quenched at a pH of 4.0, dividing FRET/mTurquoise2 avoided a mathematically incorrect division by 0.

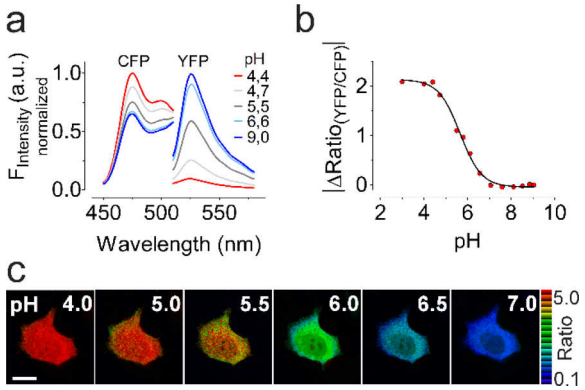

Figure 2. Imaging pH changes with pH-Lemon by separately illuminating mTurquoise2 and EYFP. (a) Emission spectra of mTurquoise2 and EYFP of pH-Lemon at different pH values *in vitro*. FPs were illuminated at 413 and 480 nm, respectively. (b) Concentration response curve of ratio signals of mTurquoise2 and EYFP of purified pH-Lemon upon separate excitation. Data of *in vitro* measurements represent n = 3 ± SD. (c) Representative, pseudocolored high resolution ratio (mTurquoise2 fluorescence/EYFP fluorescence) images of HeLa cells expressing cytosolic pH-Lemon. Images were generated using ACLSM. Cells were illuminated with 445 nm laser light to excite mTurquoise2 and then at 514 nm laser light to excite EYFP directly. Scale bar represents 10 μm.

RESULTS AND DISCUSSION

Based on the principle of pHlameleon,[27] we generated a novel biosensor that builds on the pH stable mTurquoise2[31] and the highly pH sensitive EYFP[29] (Figure 1a,b and SI Figure S-1a). The fluorescence of mTurquoise2 remained stable over a considerable range of pH values (Figure 1a). The pH-sensitive EYFP, however, already displayed high pH sensitivity and, thus, a significant loss of fluorescence intensity of 50% at pH 6.3. Moreover, at pH 4.0, the fluorescence intensity of EYFP was almost quenched up to 100% (Figure 1a). Since the new sensor is based on the bright yellow pH sensitive EYFP, we named it pH-Lemon. Analogously to the pHlameleon principle,[27] pH-Lemon represents a ratiometric pH sensor, that consists of two, via a flexible GGGGS linker, closely fused, differently colored FPs to yield high FRET ratio signals at neutral to alkaline pH values (Figure 1b). Due to the pH sensitivity of the FRET acceptor, we expected the FRET ratio signal of pH-Lemon to decrease upon acidification (Figure 1b). Investigation of cells expressing pH-Lemon that were treated with nigericin and monensin and exposed to extracellular solutions of different pH allowed the observation

DOI: 10.1021/acssensors.8b01599
ACS Sens. 2019, 4, 883−891

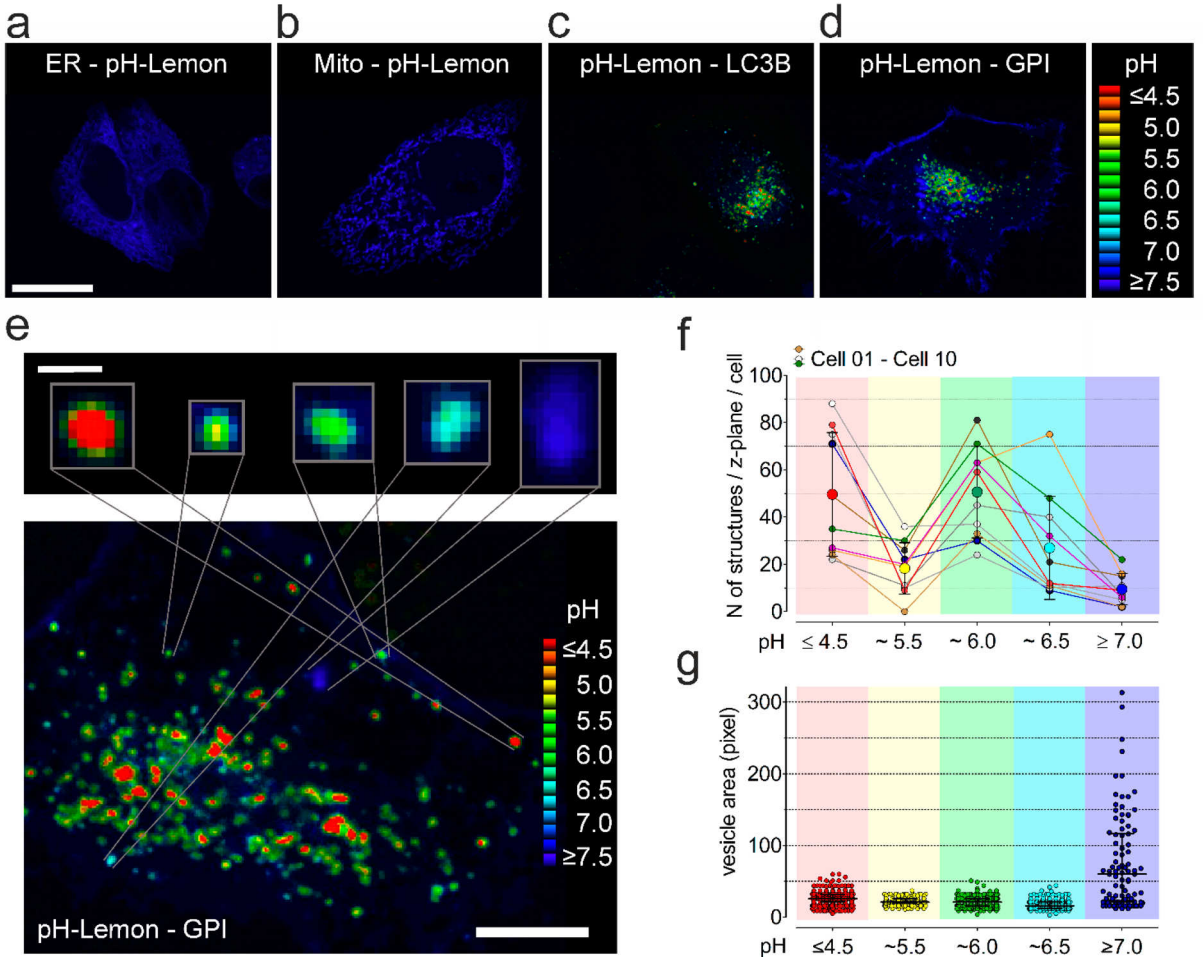

Figure 3. High-resolution imaging (ACLSM) of organelle targeted pH-Lemon. Representative pseudocolor ratio image ($F_{mTurquoise2}/F_{EYFP}$) of HeLa cells expressing pH-Lemon targeted into (a) the ER lumen, (b) the mitochondrial matrix, (c) fused to LC3B to target pH-Lemon to autophagosomes and autophagolysosomes, or (d) a GPI-anchor. Scale bar represents 10 μm. (e) Zoom images of pH-Lemon − GPI revealing the different colored vesicles with distinct ratio values, i.e., pH levels. Scale bar in upper panel represents 1 μm, in lower panel 10 μm. (f) $X-Y$ plot showing the number of intracellular structures with defined ratio values, i.e., pH levels per z-plane of individual HeLa cells (small dots, n = 10 cells). Large dots represent average ± SEM. Connections by thin lines represent 1 cell. (g) Comparison of the vesicle area (in pixel) of different colored vesicles. Data represents median ± interquartile ranges, n = 10 cells, 1550 vesicles were analyzed in total.

of large pH-dependent, ratiometric changes of the FRET-ratio (Figure 1c−e). The half maximal effective concentration (EC_{50}) of the pH dependent changes in FRET ratios was 6.3 (6.27−6.35) *in situ* (Figure 1f and Figure S-1b). Compared to SypHer (Figure 1f), another genetically encoded pH biosensor, pH-Lemon displayed a significantly higher sensitivity throughout the neutral-to-acidic pH range. It was demonstrated earlier that mTurquoise2 is suitable as a FRET-donor for multiple acceptors. Since mTurquoise2 has an extremely low pK_a and a higher brightness, as well as higher lifetime compared to other cyan FPs, the use of mTurquoise2 seems highly advantageous.[28,31,32] However, the pH-sensitivity of pH-Lemon and pHlameleons might further be adjusted by mutations or exchanging the FRET-acceptor, EYFP, for another FP variant.

For further characterization *in vitro* on a plate reader we purified bacterially expressed pH-Lemon. Figure 1g shows the emission spectra of purified pH-Lemon at different pH values upon excitation of the FRET donor, i.e., mTurquoise2. In line with our findings in intact cells, acidification reduced the FRET signal and consequently increased mTurquoise2 fluorescence of pH-Lemon (Figure 1g,h). The EC_{50} of the recombinant construct was 5.4 (5.3−5.46) (Figure 1h). The higher pK_a values *in situ* might be due to the intracellular, protein-rich environment, or limited H^+ cell-permeability. The strong pH sensitivity of the purified pH-Lemon remained unaffected by increasing the temperature up to 45 °C (Figure S-1c), pointing to the temperature stability of the probe. As depicted in Figure 1b, in pH-Lemon, the C-terminus of mTurquoise2 was fused to the N-terminus of EYFP via a small, flexible linker to yield high FRET. To verify whether the sequential order of the FPs has an impact on the FRET efficiency we constructed an analogous construct in which the N-terminus of mTurquoise2 was fused to the C-terminus of EYFP (Figure S-1d). This approach increased the dynamic range (Figure S-1d and e), with an EC_{50} of 6.2 (6.18−6.32) (Figure S-1f). Next we tested whether an additional mTurquoise2 on the C-terminus of mTurquoise2-EYFP to yield a triple FP sensor (Figure S-1g) would further increase the dynamic range. Unexpectedly, the FRET signal of this construct was very low (Figure S-1h). Fluorescence lifetime imaging microscopy (FLIM) of HEK-293 cells expressing mTurquoise2 or pH-Lemon confirmed the pH stability of mTurquoise2, the functionality and the high dynamic range of the pH probe (Figure 1i).

DOI: 10.1021/acssensors.8b01599
ACS Sens. 2019, 4, 883−891

To expand the application of pH-Lemon beyond classical FRET-imaging, we next analyzed the pH sensitivity of pH-Lemon by illuminating both FPs separately (Figure 2).

Compared to FRET imaging (Figure 1) the separate excitation of the pH-stable mTurquoise2 and EYFP of pH-Lemon yielded a higher dynamic range *in vitro* (Figure 2a and b) as well as in cells using high resolution array confocal laser microscopy (ACLSM) (Figure 2c). Notably, the EC_{50} values of pH-Lemon only moderately changed upon separate excitation from 5.4 to 5.6 (Figure 2b). The fluorescence lifetime of recombinant pH-Lemon showed strong pH sensitivity confirming the principle and characteristics of the sensor (Figure S-2a). *In situ* lifetimes for pH-Lemon expressed in HEK-293 cells at different pH values were as followed: 2.477 ns ± 0.09948 ns for pH 7.01, 2.818 ns ± 0.1501 ns for pH 6.05, and 3.686 ns ± 0.117 ns for pH 4.03 (Figure S-2b–h). These experiments emphasize that pH-Lemon is well suited to quantify pH levels and fluctuations in living cells exploiting all advantages of the FLIM technology.[33] Next we performed a series of live-cell-imaging experiments in subcellular locations using differentially targeted pH-Lemons (Figure 3a–d). As expected, pH-Lemon targeted to the endoplasmic reticulum (ER) (Figure 3a), the mitochondrial matrix (Figure 3b), the outermitochondrial membrane (Figure S-3a), or the cytoplasm (Figure S-3b) displayed a clear neutral to alkaline pH-value within these organelles. Because saturation of the biosensor at and above pH 7.5 apparently does not allow discrimination between neutral and alkaline environment (Figure 2b and c), the ratio signals and, therefore, the pseudocolorations were similar in all of these compartments. For the observation of pH values in autophagosomes, autolysosomes, and lysosomes, we generated a pH-Lemon version using the well-known autophagy marker LC3B.[34] LC3B is important in the initial formation of autophagosomes, also called phagophores. During the following fusion of mature autophagosomes with lysosomes, LC3B contacts the acidic lysosomal lumen.[34,35] Interestingly, in nutrient-starved HeLa cells expressing the autolysosomal targeted pH-Lemon - LC3B, we could detect a clear heterogeneity among vesicles ranging from strongly acidic to neutral pH levels with the more acidic vesicles clustering in the perinuclear region (Figure 3c).

These experiments clearly indicate, that pH-Lemon − LC3B represents a valuable tool to investigate autophagic vesicle maturation or turnover at the level of individual cells. Another pH-sensor was created by fusing pH-Lemon to the glycophosphatidylinositol (GPI) anchor peptide[36] that targets pH-Lemon to the lumen of the Golgi apparatus, the inside of the secretory vesicles emanated from the Golgi, and finally (outwardfacing) the plasma membrane (Figure 3d). The appropriate targeting of pH-Lemon − GPI to the secretory pathway was confirmed in cells coexpressing pH-Lemon − GPI and mCherry-Golgi-7 (Figure S-3c). An overlay of the mTurquoise2 fluorescence image of pH-Lemon − GPI with the red fluorescent Golgi plasmid revealed a high colocalization in the Golgi as well as the GPI-positive vesicles (Figure S-3c). As expected, a fraction of pH-Lemon could be seen on the plasma membrane as well (Figures 3d, S-3c–g), indicating that the sensor successfully traversed the entire anterograde secretory pathway. Upon entering the secretory pathway, pH-Lemon − GPI revealed many intracellular acidic vesicles in HeLa (Figure 3d and e), as well as INS-1 (Figure S-3d) and HEK-293 (Figure S-3e) cells. This suggests that a significant portion of pH-Lemon may be either (1) shunted from the anterograde secretory pathway directly to the endosomal–lysosomal system, for example, from the Golgi, or (2) first delivered to the plasma membrane and then recycled by endocytosis to traverse the endolysosomal system. Interestingly, HEK-293 cells expressing pH-Lemon − GPI possessed numerous large acidic vesicles when imaged using either ACLSM (Figure S-3b) or FLIM (Figure S-4a and d). These findings might point to greater interaction between the secretory and endosomal compartments in HEK-293 cells. In HeLa cells expressing pH-Lemon − GPI we could classify vesicular structures with distinct fluorescence ratio values ($F_{mTurquoise2}/F_{EYFP}$). These structures include (I) vesicles with different diameters with a red, i.e., very acidic (pH ≤ 4.5) lumen; (II) smaller vesicles with a yellow, i.e., pH ∼ 5.5 lm; (III) very small vesicles with a green lumen, i.e., pH 6.0; (IV) some homogeneous cyan structures, i.e., pH ∼ 6.5 of variable sizes; and (V) larger homogeneous dark blue areas, representing parts of the Golgi complex with an estimated pH of around 7.0 (Figure 3e–g). Thus, it remains unclear, which of these vesicles belong to the secretory or lysosomal systems. Additional experiments are required to determine their precise identities with specific subcellular compartments. However, by expressing pH-Lemon − GPI, we were able to reveal huge variability of different pH values throughout these important pathways. That these represent distinct vesicle species as opposed to variability in probe concentration is supported by our finding that the total fluorescence (i.e., sum of CFP and YFP fluorescence) of the probe did not correlate with the respective ratio signals of the distinct vesicles/structures (Figure S-3f). Notably, most red and yellow vesicles showed a green border (Figure 3e) which might result from resolution limitations or vesicle movement within the cell, rather than reflect pH variations within such vesicles. To exclude possible imaging artifacts, we also used FLIM of pH-Lemon − GPI expressed in HEK-293 cells. These experiments showed that the fluorescence lifetime of pH-Lemon − GPI in distinct vesicles varied between 2.2 and 3.5 ns confirming the huge variability of pH values among these subcellular structures (Figure S-4d–f). Interestingly, in the enlarged vesicles of HEK cells, the FLIM measurements also showed lower pH values at the vesicle border (Figure S-4d). One interesting possibility to explain these huge structures with clearly heterogeneous ratio signal is that they might represent multivesicular bodies, containing distinct suborganelle pH values, or the signal might be caused by previously unknown microheterogeneity.[37] However, the vesicular border might also be caused by resolution limitations. In order to eliminate the possibility that the pH sensitive EYFP is degraded, which would, therefore, show an extremely high ratio signal (i.e., red color), we treated cells with a mixture of sodium azide (NaN_3) and ammonium chloride (NH_4Cl). The combination of these compounds was shown to efficiently neutralize acidic compartments.[38] Addition of NaN_3/NH_4Cl instantly neutralized most of the acidic vesicles that was accompanied by a decrease of the ratio signal and a clear increase of EYFP fluorescence (Figure S-3g), demonstrating that pH-Lemon − GPI remained stable and functional in such acidic vesicles. To investigate the pH-value of vesicles of the endosomal secretory and lysosomal pathway over time, we imaged pH-Lemon − GPI using a fluorescence wide-field imaging system (Figure 4). Although the spatial resolution of this imaging system is considerably lower than that of the array confocal microscope (Figure 3 and Figure S-3), we could clearly detect vesicles with distinct ratio

DOI: 10.1021/acssensors.8b01599
ACS Sens. 2019, 4, 883–891

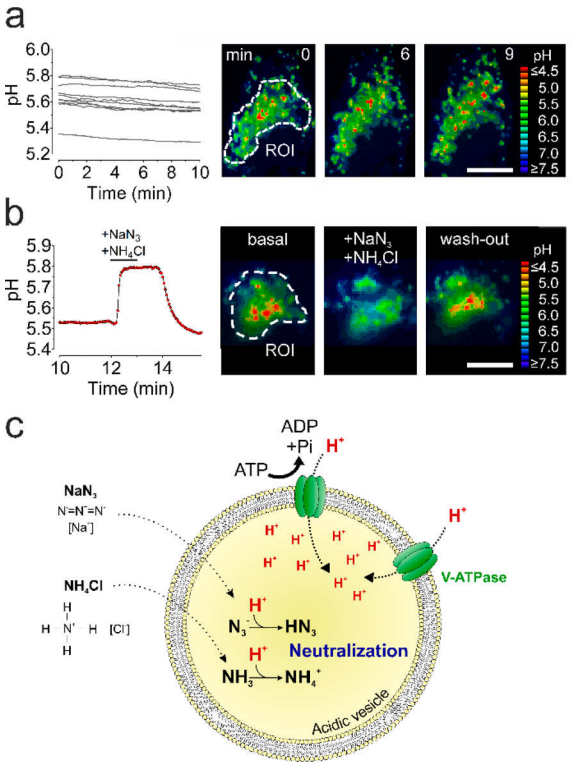

Figure 4. Wide-field time-lapse fluorescence imaging of pH-Lemon − GPI. (a) Representative time course (left panel) and images (right panel) of estimated pH values in the vesicular regions (ROIs) (n = 10, left panel) over time of HeLa cells expressing pH-Lemon − GPI. Cells were imaged every 3 s. Scale bars represent 10 μm. (b) Representative time course (left panel) and images (right panel) of the effect of the addition and removal of a neutralizing buffer containing of 0.5% (w/v) NaN_3 and 50 mM NH_4Cl to acidic vesicles in HeLa cells expressing pH-Lemon − GPI. Cells were imaged every 3 s. Scale bars represent 10 μm. (c) Schematic illustration of a cellular vesicle that acidifies its lumen via V-ATPases, ATP-consuming proton pumps located in the vesicular membrane. NaN_3 and NH_4Cl are proposed to diffuse through the vesicular membrane, causing neutralization.

values (Figure 4a,b, Movie S-1−4). After a short, transient addition of NaN_3 and NH_4Cl, the vesicles were rapidly neutralized, followed by a reacidification of the vesicles (Figure 4b). NaN_3 and NH_4Cl might diffuse through the vesicular membrane to buffer the protons in the vesicular lumen (Figure 4c). Time-lapse imaging further revealed a high mobility of the acidic vesicles, whereas the ratio signal, i.e., luminal pH, remained relatively constant over minutes. Considering the mild decrease of the ratio signals, it was not possible to discriminate between a low photobleaching effect or an acidification due to mild starvation, since the cells were kept and imaged in "2Ca"-buffer without any amino acids or nutrients (Figure 4a and Movie S-1). Stimulation of the cells with ATP, an inositol 1,4,5-trisphosphate-generating (IP_3) agonist that mobilizes ER-Ca^{2+} did not considerably affect the ratio signals of pH-Lemon − GPI, but strongly decelerated vesicle movements (Figure S5a and Movie S-2). To transform FRET-ratio signals to actual pH-values, we calibrated pH-Lemon − GPI in HeLa cells using the respective ratio signals on the cell surface upon treatment with extracellular buffers (see Experimental Section). Interestingly, the acidic pH value of vesicles remained almost unaffected by the addition of an alkaline experimental buffer with a pH of 10.0, while a switch to extracellular pH of 4.0 immediately further acidified intracellular vesicles (Figure S-5b and Movie S-3). Such effects might be cell type specific and may depend on the presence of H^+/ion exchangers, channels, or pumps.

We then used intact HeLa cells expressing pH-Lemon − GPI to test the pH dynamics of acidic vesicle in response to a short transient addition of NaN_3/NH_4Cl (Figure 4b and Movie S-4). The pH of all vesicles was rapidly elevated upon the addition of these compounds. Interestingly, the acidic pH of intracellular vesicles was fully reestablished after the removal of NaN_3/NH_4Cl within approximately 5 min (Figure 4b and Movie S-4). These experiments demonstrated the suitability of pH-Lemon to quantitatively visualize pH dynamics of cellular organelles with high temporal resolution. Compared to the commonly used LysoTracker Red DND-99,[25] which is irreversibly lost upon vesicle neutralization (Figure S-5c), pH-Lemon − GPI remains functionally intact within organelles of the endosomal and lysosomal pathway (Figure 4b), pointing to an important advantage of this genetically encoded pH biosensor. We further tested pH-Lemon − GPI for its suitability to report vesicular pH neutralization upon a treatment of cells with bafilomycin-A, a prominent inhibitor of vacuolar-type H^+ ATPase (V-ATPase). As expected, bafilomycin-A significantly increased the intravesicular pH (Figure S-6a,b).[39−41]

Compared to control cells, cells treated with bafilomycin-A were unable to reacidify intracellular vesicles after NaN_3/NH_4Cl wash-out, due to inhibition of the V-ATPase (Figure S-6a and c−f), while vesicles significantly reacidified in control cells (Figure S-6c−f).[42] In future, pH-Lemon might represent a valuable tool to study pharmacological compounds and their effect on vesicular pH-dynamics. In conclusion, our data demonstrate a novel FRET-based biosensor, pH-Lemon, that represents a suitable pH reporter for the quantitative high-resolution visualization of pH changes between pH 4.0 and pH 7.0 in different biological samples and models.

Since several diseases are correlated with altered cellular pH,[43−46] the estimation and time lapse imaging of these pH changes is of great importance. Furthermore, subcellular pH changes are also produced by key metabolic activities in healthy cells. Hence, besides employment as a pH reporter of cellular organelles, targeted pH-Lemon could therefore be exploited to determine global and local rates of (an-) aerobic glycolysis, lipolysis, and mitochondrial respiration on the level of individual cells.

■ ASSOCIATED CONTENT

Supporting Information

The Supporting Information is available free of charge on the ACS Publications website at DOI: 10.1021/acssensors.8b01599.

Cloning strategies for the generation of pH-Lemon constructs; Cell culture and transfection of HEK-293 cells for FLIM imaging; Calibration of pH-Lemon − GPI; Primers used to generate pH-Lemon constructs; Nucleotide sequences for cloning different pH-Lemon constructs; Characterization of mTurquoise2, EYFP, and fusion constructs of both fluorescent protein; FLIM characterization of pH-Lemon; ACLSM visualization of pH-Lemon; FLIM of HEK-293 cells expressing pH-Lemon − GPI; (PDF)

DOI: 10.1021/acssensors.8b01599
ACS Sens. 2019, 4, 883−891

Movie S-1: Real-time imaging of pH-Lemon − GPI in HeLa cells over 10 min (AVI)

Movie S-2: Elevated cytosolic Ca^{2+} levels due to addition of an IP3-generating agonist in pH-Lemon − GPI expressing HeLa cells (AVI)

Movie S-3: Effects of extracellular, nonpermeabilizing buffer change on the vesicular pH of GPI vesicles (AVI)

Movie S-4: Addition of sodium azide and ammonium chloride to neutralize acidic vesicles in HeLa cells (AVI)

AUTHOR INFORMATION

Corresponding Authors

*E-mail: sandra.burgstaller@medunigraz.at (S. B.).
*E-mail: helmut.bischof@medunigraz.at (H. B.).
*E-mail: markus.weiermair@medunigraz.at (M. W.-W.).
*E-mail: wolfgang.graier@medunigraz.at (W. F. G.).
*E-mail: roland.malli@medunigraz.at (R. M.).

ORCID

Roland Malli: 0000-0001-6327-8729

Author Contributions

S. Bu. designed and cloned the pH-Lemon constructs, performed experiments, analyzed all data and wrote the manuscript. H.B., B.G., and J.R.-M. assisted in data analysis; E.E., M.W.-W., and J.C.H. contributed to the experimental design; S.S. and T.M. performed protein expression and purification; T.G. S. Ba. and A.B. performed FLIM experiments; R.R. assisted with cell culture; W.F.G. together with R.M. supervised the project and wrote the manuscript.

Notes

The authors declare no competing financial interest.

ACKNOWLEDGMENTS

We thank C.B. Newgard, Department of Pharmacology and Cancer Biology, Duke University School of Medicine, USA, for providing us with INS-1 832/13 cells. We thank Michael Davidson (National High Magnetic Field Laboratory, Florida, USA) for mCherry-Golgi-7. The authors further acknowledge Sandra Blass and Anna Schreilechner for the excellent technical support and the scientific advisory board of Next Generation Fluorescence Imaging (NGFI) GmbH (http://www.ngfi.eu/), a spin-off company of the Medical University of Graz. The research was funded by the Ph.D. program Molecular Medicine (MOLMED) of the Medical University of Graz, by Nikon Austria within the Nikon-Center of Excellence, Graz, the Austrian Science Fund (FWF) projects I3716−B27 and P28529−B27 to R.M., the doctoral program Metabolic and Cardiovascular Disease (DK-W1226), and P27070 to W.F.G. The Nikon Center of Excellence, Graz, is supported by the Austrian infrastructure program 2013/2014, Nikon Austria Inc., and BioTechMed, Graz. This work was partly supported by the President's International Fellowship Initiative of CAS (No. 2015VBB045), the National Natural Science Foundation of China (No. 31450110423), the Austrian Science Fund (FWF: P28854 and I3792), the Austrian Research Promotion Agency (FFG: 864690), the Integrative Metabolism Research Center Graz, the Austrian infrastructure program 2016/2017, BioTechMed/Graz, and the OMICS center Graz to T. M.

REFERENCES

(1) Alberty, R. A Kinetic effects of the ionization of groups in the enzyme molecule. *J. Cell. Comp. Physiol.* **1956**, *47*, 245−281.
(2) Tamai, I.; Yabuuchi, H.; Nezu, J.; Sai, Y.; Oku, A.; Shimane, M.; Tsuji, A. Cloning and characterization of a novel human pH-dependent organic cation transporter, OCTN1. *FEBS Lett.* **1997**, *419*, 107−111.
(3) Eriksen, J.; Chang, R.; McGregor, M.; Silm, K.; Suzuki, T.; Edwards, R. H. Protons Regulate Vesicular Glutamate Transporters through an Allosteric Mechanism. *Neuron* **2016**, *90*, 768−780.
(4) Coulter, K. L.; Périer, F.; Radeke, C. M.; Vandenberg, C. A. Identification and molecular localization of a pH-sensing domain for the inward rectifier potassium channel HIR. *Neuron* **1995**, *15*, 1157−1168.
(5) Han, J.-E.; Cho, J.-H.; Choi, I.-S.; Kim, D.-Y.; Jang, I.-S. Effects of acidic pH on voltage-gated ion channels in rat trigeminal mesencephalic nucleus neurons. *Korean J. Physiol. Pharmacol.* **2017**, *21*, 215−223.
(6) Vullo, S.; Bonifacio, G.; Roy, S.; Johner, N.; Bernèche, S.; Kellenberger, S. Conformational dynamics and role of the acidic pocket in ASIC pH-dependent gating. *Proc. Natl. Acad. Sci. U. S. A.* **2017**, *114*, 3768−3773.
(7) Mikles, D. C.; Bhat, V.; Schuchardt, B. J.; Deegan, B. J.; Seldeen, K. L.; McDonald, C. B.; Farooq, A. pH modulates the binding of early growth response protein 1 transcription factor to DNA. *FEBS J.* **2013**, *280*, 3669−3684.
(8) Madshus, I. H. Regulation of intracellular pH in eukaryotic cells. *Biochem. J.* **1988**, *250*, 1−8.
(9) Dechant, R.; Peter, M. Cytosolic pH: A conserved regulator of cell growth? *Molecular & Cellular Oncology* **2014**, *1*, e969643.
(10) Santo-Domingo, J.; Demaurex, N. Perspectives on: SGP symposium on mitochondrial physiology and medicine: the renaissance of mitochondrial pH. *J. Gen. Physiol.* **2012**, *139*, 415−423.
(11) Hu, Y.-B.; Dammer, E. B.; Ren, R.-J.; Wang, G. The endosomal-lysosomal system: from acidification and cargo sorting to neurodegeneration. *Transl. Neurodegener.* **2015**, *4*, 18.
(12) Wileman, T. Autophagy as a defence against intracellular pathogens. *Essays Biochem.* **2013**, *55*, 153−163.
(13) Schmidt, W. K.; Moore, H. P. Ionic milieu controls the compartment-specific activation of pro-opiomelanocortin processing in AtT-20 cells. *Mol. Biol. Cell* **1995**, *6*, 1271−1285.
(14) Huotari, J.; Helenius, A. Endosome maturation. *EMBO J.* **2011**, *30*, 3481−3500.
(15) DiCiccio, J. E.; Steinberg, B. E. Lysosomal pH and analysis of the counter ion pathways that support acidification. *J. Gen. Physiol.* **2011**, *137*, 385−390.
(16) Johnson, D. E.; Ostrowski, P.; Jaumouillé, V.; Grinstein, S. The position of lysosomes within the cell determines their luminal pH. *J. Cell Biol.* **2016**, *212*, 677−692.
(17) Breton, S.; Brown, D. Regulation of luminal acidification by the V-ATPase. *Physiology* **2013**, *28*, 318−329.
(18) Pérez-Sayáns. Role of V-ATPases in solid tumors: Importance of the subunit C (Review). *Int. J. Oncol.* **2009**, *34*, 1 DOI: 10.3892/ijo_00000280.
(19) Hu, Y.-B.; Dammer, E. B.; Ren, R.-J.; Wang, G. The endosomal-lysosomal system: from acidification and cargo sorting to neurodegeneration. *Transl. Neurodegener.* **2015**, *4*, 1 DOI: 10.1186/s40035-015-0041-1.
(20) Mauvezin, C.; Nagy, P.; Juhász, G.; Neufeld, T. P. Autophagosome-lysosome fusion is independent of V-ATPase-mediated acidification. *Nat. Commun.* **2015**, *6*, 7007.
(21) Mindell, J. A. Lysosomal acidification mechanisms. *Annu. Rev. Physiol.* **2012**, *74*, 69−86.
(22) Hou, J.-T.; Ren, W. X.; Li, K.; Seo, J.; Sharma, A.; Yu, X.-Q.; Kim, J. S. Fluorescent bioimaging of pH: from design to applications. *Chem. Soc. Rev.* **2017**, *46*, 2076−2090.
(23) Han, J.; Burgess, K. Fluorescent indicators for intracellular pH. *Chem. Rev.* **2010**, *110*, 2709−2728.
(24) Fernández, A.; Vendrell, M. Smart fluorescent probes for imaging macrophage activity. *Chem. Soc. Rev.* **2016**, *45*, 1182−1196.
(25) Pierzyńska-Mach, A.; Janowski, P. A.; Dobrucki, J. W. Evaluation of acridine orange, LysoTracker Red, and quinacrine as

DOI: 10.1021/acssensors.8b01599
ACS Sens. 2019, 4, 883−891

fluorescent probes for long-term tracking of acidic vesicles. *Cytometry, Part A* **2014**, *85*, 729−737.
(26) Miesenböck, G.; de Angelis, D. A.; Rothman, J. E. Visualizing secretion and synaptic transmission with pH-sensitive green fluorescent proteins. *Nature* **1998**, *394*, 192−195.
(27) Esposito, A.; Gralle, M.; Dani, M. A. C.; Lange, D.; Wouters, F. S. pHlameleons: a family of FRET-based protein sensors for quantitative pH imaging. *Biochemistry* **2008**, *47*, 13115−13126.
(28) Rizzo, M. A.; Springer, G. H.; Granada, B.; Piston, D. W. An improved cyan fluorescent protein variant useful for FRET. *Nat. Biotechnol.* **2004**, *22*, 445−449.
(29) Kremers, G.-J.; Goedhart, J.; van Munster, E. B.; Gadella, T. W. J. Cyan and yellow super fluorescent proteins with improved brightness, protein folding, and FRET Förster radius. *Biochemistry* **2006**, *45*, 6570−6580.
(30) Rupprecht, C.; Wingen, M.; Potzkei, J.; Gensch, T.; Jaeger, K.-E.; Drepper, T. A novel FbFP-based biosensor toolbox for sensitive in vivo determination of intracellular pH. *J. Biotechnol.* **2017**, *258*, 25−32.
(31) Goedhart, J.; von Stetten, D.; Noirclerc-Savoye, M.; Lelimousin, M.; Joosen, L.; Hink, M. A.; van Weeren, L.; Gadella, T. W.J.; Royant, A. Structure-guided evolution of cyan fluorescent proteins towards a quantum yield of 93%. *Nat. Commun.* **2012**, *3*, 751.
(32) Heim, R.; Prasher, D. C.; Tsien, R. Y. Wavelength mutations and posttranslational autoxidation of green fluorescent protein. *Proc. Natl. Acad. Sci. U. S. A.* **1994**, *91*, 12501−12504.
(33) Becker, W. Fluorescence lifetime imaging−techniques and applications. *J. Microsc.* **2012**, *247*, 119−136.
(34) Klionsky, D. J.; Abdelmohsen, K.; Abe, A.; Abedin, M. J.; Abeliovich, H.; Acevedo Arozena, A.; Adachi, H.; Adams, C. M.; Adams, P. D.; Adeli, K. Guidelines for the use and interpretation of assays for monitoring autophagy (3rd edition). *Autophagy* **2016**, *12*, 1−222.
(35) Nakamura, S.; Yoshimori, T. New insights into autophagosome-lysosome fusion. *J. Cell Sci.* **2017**, *130*, 1209−1216.
(36) Zurzolo, C.; Simons, K. Glycosylphosphatidylinositol-anchored proteins: Membrane organization and transport. *Biochim. Biophys. Acta, Biomembr.* **2016**, *1858*, 632−639.
(37) Piper, R. C.; Katzmann, D. J. Biogenesis and Function of Multivesicular Bodies. *Annu. Rev. Cell Dev. Biol.* **2007**, *23*, 519−547.
(38) Marchetti, A.; Lelong, E.; Cosson, P. A measure of endosomal pH by flow cytometry in Dictyostelium. *BMC Res. Notes* **2009**, *2*, 7.
(39) Yoshimori, T.; Yamamoto, A.; Moriyama, Y.; Futai, M.; Tashiro, Y. Bafilomycin A1, a specific inhibitor of vacuolar-type H(+)-ATPase, inhibits acidification and protein degradation in lysosomes of cultured cells. *J. Biol. Chem.* **1991**, *266*, 17707−17712.
(40) Lafourcade, C.; Sobo, K.; Kieffer-Jaquinod, S.; Garin, J.; van der Goot, F. G. Regulation of the V-ATPase along the Endocytic Pathway Occurs through Reversible Subunit Association and Membrane Localization. *PLoS One* **2008**, *3*, e2758.
(41) Maxson, M. E.; Grinstein, S. The vacuolar-type H^+-ATPase at a glance - more than a proton pump. *J. Cell Sci.* **2014**, *127*, 4987−4993.
(42) Wang, D.; Hiesinger, P. R. The vesicular ATPase: a missing link between acidification and exocytosis. *J. Cell Biol.* **2013**, *203*, 171−173.
(43) Davies, T. A.; Fine, R. E.; Johnson, R. J.; Levesque, C. A.; Rathbun, W. H.; Seetoo, K. F.; Smith, S. J.; Strohmeier, G.; Volicer, L.; Delva, L. Non-age related differences in thrombin responses by platelets from male patients with advanced Alzheimer's disease. *Biochem. Biophys. Res. Commun.* **1993**, *194*, 537−543.
(44) Gennari, F. J. Pathophysiology of metabolic alkalosis: a new classification based on the centrality of stimulated collecting duct ion transport. *Am. J. Kidney Dis.* **2011**, *58*, 626−636.
(45) Swietach, P.; Vaughan-Jones, R. D.; Harris, A. L.; Hulikova, A. The chemistry, physiology and pathology of pH in cancer. *Philos. Trans. R. Soc., B* **2014**, *369*, 20130099.
(46) Maxfield, F. R. Role of endosomes and lysosomes in human disease. *Cold Spring Harbor Perspect. Biol.* **2014**, *6*, a016931.

DOI: 10.1021/acssensors.8b01599
ACS Sens. 2019, 4, 883−891